IEEE Access
Multidisciplinary | Rapid Review | Open Access Journal

Received June 15, 2021, accepted July 18, 2021, date of publication July 26, 2021, date of current version August 4, 2021.

*Digital Object Identifier 10.1109/ACCESS.2021.3100098*

# Corneal Biomechanics Assessment Using High Frequency Ultrasound B-Mode Imaging

**HASSAN M. AHMED[1], WALID AL-ATABANY[1,2], AND NANCY M. SALEM[1]**
[1]Department of Biomedical Engineering, Faculty of Engineering, Helwan University, Cairo 11795, Egypt
[2]Information Technology and Computer Science School, Nile University, Giza 16453, Egypt

Corresponding author: Hassan M. Ahmed (hassan.gbr@h-eng.helwan.edu.eg)

**ABSTRACT** Assessment of corneal biomechanics for pre- and post-refractive surgery is of great clinical importance. Corneal biomechanics affect vision quality of human eye. Many factors affect corneal biomechanics such as, age, corneal diseases and corneal refractive surgery. There is a need for non-invasive in-vivo measurement of corneal biomechanics due to corneal shape preserving as opposed to ex-vivo measurements that destructs corneal tissue. In this study, a new approach for assessing corneal biomechanics in-vivo non-invasively using ultrasound estimation method with 100 KHz frame rate is proposed. Three models in conjunction with each other are used to study the biomechanics behavior of corneal tissue pre- and post-refractive surgery. These three models are cornea FEM, cornea scatterrer model and ultrasound transducer model respectively. Nine different elastic moduli corneal models are constructed to achieve this goal; 140KPa, 300KPa, 600KPa and 800KPa as post-refractive surgery models and 1MPa, 1.5MPa, 2MPa, 2.5MPa and 3MPa as pre-refractive surgery models respectively. Time-To-Peak (TTP) deformation, deformation amplitude (DA), deformation amplitude ratio at 2 mm (DA ratio 2 mm) and shear wave speed (SWS) are estimated for each of the nine involved corneal models in this study. Results show that TTP is decreasing (6.9 msec. at 140KPa to 5.3 msec. at 3MPa) while increasing the elastic modulus of corneal tissue. Also, DA is decreasing (2 mm at 140KPa to 0.5 mm at 3MPa), while increasing the elastic modulus as well. However, DA ratio shows decrease while increasing of elastic modulus to reflect the difficulty of corneal tissue to deform uniformly at higher elastic moduli. Estimated SWS shows an average accuracy of 98% of the theoretical SWS.

**INDEX TERMS** Corneal biomechanics, ultrasonic biomechanics estimation, corneal post refractive surgery.

## I. INTRODUCTION

Cornea is the transparent component of human ocular system that acts as a protective part enveloping other human ocular components such as lens. It preserves shape of human eye and accounts for most of its refractive power [1], [2]. Shape, transparency and uniformity of human cornea are important factors when assessing its role to vision. However, human vision degradation is caused by cornea shape alteration due to age, corneal diseases and refractive surgery [1]. Developing post-surgery ectasia is common among patients undergoing refractive surgeries. Hence, assessing corneal biomechanics post-refractive surgery is of great importance to ophthalmologists [3]–[5]. Refractive surgery outcomes are subjective to corneal biomechanics [6]–[9].

The associate editor coordinating the review of this manuscript and approving it for publication was Jingang Jiang.

Studying corneal behavior has been extensively investigated by many models and techniques [10]. Age related factors are studied in [11]–[13]. X-Rays diffraction is used to investigate the inter-fibril spacing of stromal collagen fibrils and inter-molecular spacing of collagen molecules in [11]. The inter-fibril spacing of stromal collagen is found to be decreasing with age as reported in [12]. In the work presented in [13], diameter of collagen fibrils is observed to be age dependent, where there is a change of about 9% in subjects older than 65 years old compared to those under 65 years old. Cornea stiffness related to age is investigated in [14] and [15], where the cornea is found to be stiffer when getting older.

In terms of refractive surgery, myopic astigmatism is achieved by small-incision lenticule extraction (SMILE) [15]. SMILE is claimed to have minimal effect on corneal biomechanics compared to other refractive surgeries such as

**TABLE 1.** Mechanical Properties Of Human Cornea.

| Material Property | Value | |
|---|---|---|
| Young's modulus (range of values) | Pre-refractive (High E in MPa) | Post-refractive (Low E in KPa) |
| | 1, 1.5, 2, 2.5 and 3MPa [38] | 140, 300, 600 and 800KPa [37] |
| Poisson Ratio | 0.499 | |
| Heat Capacity at constant pressure | 2348 | |
| Thermal Conductivity | 0.21 | |
| Density | 911 | |

LASIK (laser-assisted in-situ keratomileusis) and femto-LASIK (femto-second laser-assisted in-situ keratomileusis) [16], [17]. SMILE has shown less effect on corneal biomechanics than femto-LASIK [17]. Corneal safety and sensitivity are studied in multiple studies [18]–[20]. LASEK (laser-assisted sub-epithelial keratectomy) is reported to have less effect on corneal biomechanics with minimal risk of developing ectasia as well [21]. However, some cases are reported to have corneal biomechanics alteration after performing LASEK [22]. Moreover, both LASEK and SMILE are reported to induce changes in corneal biomechanics, where SMILE has the advantage of inducing less biomechanics changes than LASEK does due to the preservation of stiffer anterior stroma [6].

Ultrasound techniques are used to estimate corneal biomechanics. The main algorithm for estimating soft tissue biomechanics is by acquiring a stack of deformed frames for the tissue along with a reference frame utilizing high frame rate B-mode imaging [23], [24]. Transient ultrasound acoustic radiation force impulse (ARFI) is applied by means of ultrasound focusing techniques [25]. This ARFI generates deformation wave inside tissue under study that alters the characteristic of tissue's mechanical properties such as, Young's modulus (E) and shear modulus ($\mu$). This induced shear wave speed is related to tissue shear modulus by Eqn. (1) & (2):

$$C = \sqrt{\frac{\mu}{\rho}} \tag{1}$$

$$\mu = \frac{E}{2(1+\vartheta)} \tag{2}$$

where C is the shear wave speed, $\mu$ is the shear modulus, $\rho$ is the density in $Kg/m3$, E is the Young's modulus and $\vartheta$ is the Poisson ratio for tissue under investigation respectively.

Supersonic Time-Of-Flight (TOF) [26], [27], Lateral Time-To-Peak (TTP) [28], [29] or cross correlation [29]–[32] algorithms are implemented to estimate the speed of the resulting tissue deformation wave; i.e. Shear Wave Speed (SWS).

Till now, there is no non-invasive technique for clinical ultrasound in-vivo device that is used to assess the corneal biomechanics as a single modality combining the pushing element and the imaging element. All available approaches are still proof of concepts and utilize two different elements, external one for generating the push and another one for capturing the deformed frames [33]. Even, these approaches do not give spatial distribution for the corneal biomechanics, instead they give a mean estimate for the whole cornea tissue area.

In our research, we propose a new technique where the same ultrasound transducer is used to generate highly localized ARFI to act as internal actuator to induce tissue deformation and to perform B-mode imaging procedure to capture the propagation of the deformation wave. In our research also, we can continuously change the investigated zone of cornea to cover the whole cornea area and to obtain a spatial distribution of cornea biomechanics.

In this paper, a 3D FEM in conjunction with 2D scatterrer model for human cornea and an ultrasound transducer model are implemented to study the effect of post-refractive surgery on the biomechanics of corneal tissue using ultrasound B-mode imaging. Different elastic moduli are assigned to the 3D FEM to simulate different cornea tissue biomechanics [1], [27], [34], [35]. Cornea dimensions are adopted from medical literature for average human cornea [36], [37].

The paper is organized as follows, section I gives an introduction about the cornea, their biomechanics effect and related refractive surgeries, and a brief survey on ultrasound techniques used for assessing corneal biomechanics. Section II shows a full description for the proposed approach. Section III describes the methodology of how the three proposed models interact with each other and the acquisition sequence and the shear wave speed estimation method. Experimental results are reported in section V. Finally, discussion and conclusion are presented in sections VI and VII respectively.

## II. THE PROPOSED APPROACH

Our proposed system is visualized in Fig. 1(a) where the ultrasound transducer is used on top of the human eye lid [38]. The same ultrasound transducer is used to generate the ARFI and to perform the B-mode imaging procedure. The ultrasound transducer will be fixed in the same position during the whole corneal biomechanics estimation process. At the beginning of the estimation process, the transducer is used to generate the ARFI at the corneal apex, then the ordinary B-mode imaging procedure is initiated to capture the departing deformation wave across the lateral direction.

The proposed algorithm for estimating corneal biomechanics for each elastic modulus is presented in the block diagram shown in Fig. 1(b). It shows three main blocks: First block resembles the mechanical model of the cornea, the second resembles the ultrasound transducer model and the

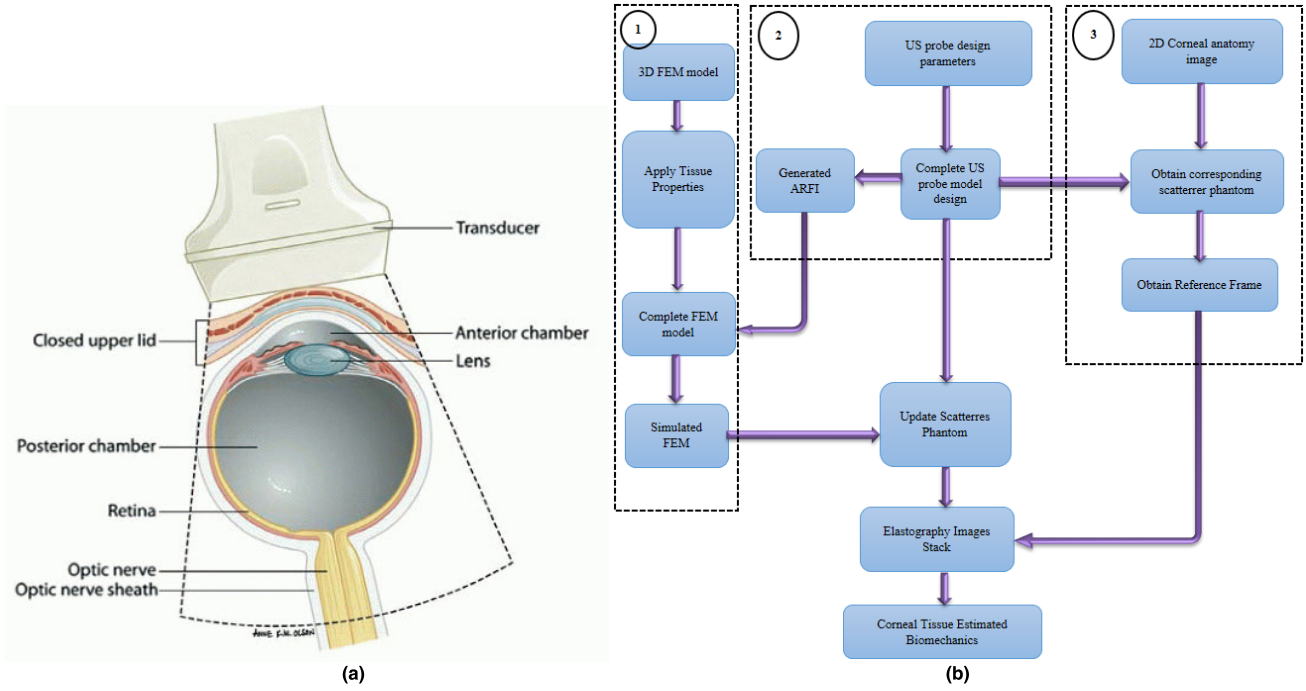


**FIGURE 1.** Block diagram of the proposed approach.

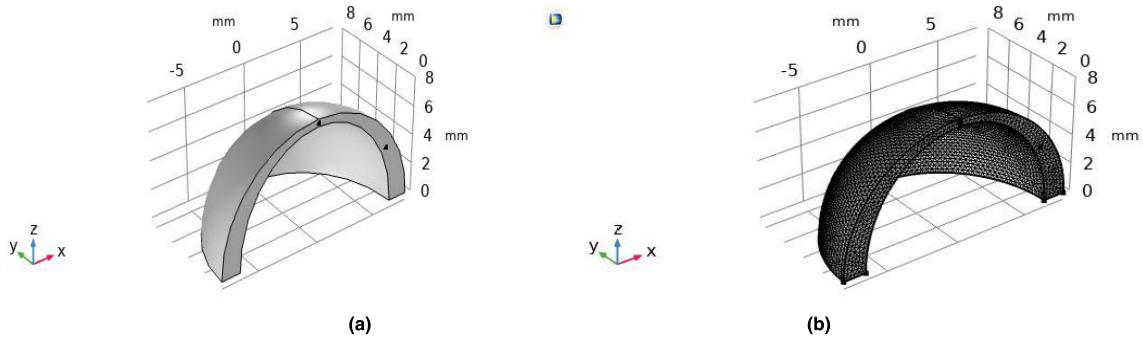


**FIGURE 2.** (a) Vertical cross section of human cornea 3D FEM, (b) Its corresponding Mesh.

third resembles the scatterrer model of the cornea. The three models are mutually interacting with each other to produce a deformed video stack of the cornea.

### A. CORNEA MECHANICAL FEM

A vertical cross section for the human cornea is modeled as 3D FEM and shown in Fig. 2 (a). The model dimensions are assigned to be equal to those of average human cornea 440 $\mu$m to 650 $\mu$m with an average of 540$\pm$30 $\mu$ m [40, 41]. The mechanical properties are set to those of cornea pre- and post-refractive surgery and are listed in Table 1. Triangular mesh is used by COMSOL software to mesh the volume of the cornea model. The mesh is set to be narrower at the volume of interest for obtaining accurate results and wider at the remaining volume to speed up the processing time. The cornea mesh is shown in Fig. 2 (b).

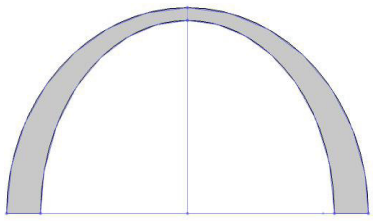

**FIGURE 3.** Cornea 2D plan view.

### B. FEM DRAWING

Human cornea is modeled using FEM as a vertical cross section to simulate its behavior for pre- and post-refractive surgery. As a consequence, corneal biomechanics changes from pre-refractive to post-refractive surgery in terms of Young's modulus. This change affects cornea behavior to external applied forces. The FEM is constructed from two

**TABLE 2.** Geometrical Dimensions of Human Cornea.

| | Circle 1 | Ellipse |
|---|---|---|
| Radius (mm) | 8 | A = 6.5, B = 7.5 |
| Sector Angle (degrees) | 180 | 180 |

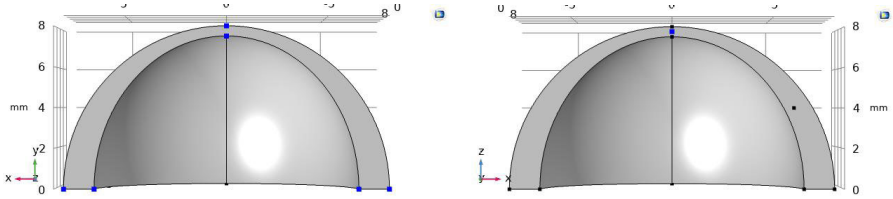


(a) (b)

**FIGURE 4.** a) Fixed boundaries as iris ciliary muscle, b) Focal point where ultrasound transient force is applied.

**TABLE 3.** Ultrasound transducer parameters.

| Parameter | Value |
|---|---|
| Center frequency (fo) | 12 MHz |
| Number of elements | 192 |
| Number of active elements | 128 |
| Elements' width | 170 µm |
| Kerf | 30 µm |
| Focal depth | 28.5 mm |

intersecting shapes, a circle and an ellipse in the 2D plan. Then the intersection is revolved around the z-axis to construct the volume of the model. Complete model in 2D plane drawing is presented in Fig. 3 and its dimensions are listed in Table 2.

### C. FEM SOLID MECHANICS

Isotropic linear visco-elastic approach is adopted for this model as it simulates Kelvin-Voigt mathematical model efficiently in Finite Element Analysis (FEA) software. Peak ARFI is applied at the apex of the cornea which is set to be at the focal point of the ultrasound beam. The fixed boundaries simulating the behavior of the ciliary muscles of cornea are set to be in the lower face of the cornea at 6 vertex points. This is shown in Fig. 4.

### D. ULTRASOUND TRANSDUCER MODEL

Ultrasound transducer is used to generate the internal push inside the cornea tissue that induces tissue deformation. As well it is used to perform B-mode imaging on the deformed tissue at subsequent time stamps to capture the propagation of the deformation wave. Therefore, the ultrasound transducer performs two functions in the transient elastography procedure, internal actuator for inducing tissue deformation and imaging to capture the induced displacement propagation.

In this model, two toolboxes in MATLAB are used to simulate the behavior of the ultrasound transducer in both cases of generating the ARFI and performing the B-mode linear imaging procedure. FOCUS toolbox is used for simulating the ultrasound transducer while generating the ARFI. However, Field II toolbox is used for simulating the ultrasound transducer imaging procedure. The transducer parameters used in both simulations are listed in Table 3.

The purpose of the ARFI is to generate a highly localized ultrasound push inside the tissue. This localization gives rise to quantitative estimation of tissue's mechanical properties. The imparted ultrasonic power due the focused push dampens highly around the focal push location in all direction exponentially. The generated ARFI induces cornea tissue to deform yielding a deformation (displacement) wave that propagates away from the focal point. The generated wave is considered to be the shear wave.

Fast Near field Method (FNM) method from FOCUS toolbox is used to simulate the ultrasound linear transducer behavior while generating the ARFI. Pressure map is simulated for the ultrasound transducer and is presented in Fig. 5. The focal point is set to be around 28.5 mm in the axial direction (depth direction). The focal point is that point where the peak ultrasound pressure generated from the transducer is applied inside the tissue. It is the imparted ultrasonic pressure that is responsible for inducing the tissue deformation and hence the shear wave. We have simulated the transducer 2D pressure map, transverse cross-sectional pressure

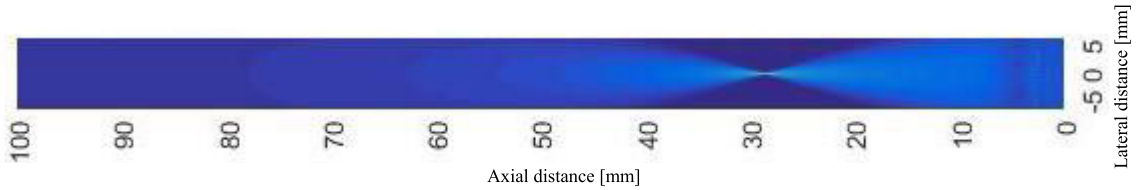


**FIGURE 5.** Simulated 2D pressure map for ultrasound transducer model.

distribution across the 2D map at different axial depths, focal axial pressure at the center and the average axial pressure. In addition, focal axial intensity, average axial intensity, focal axial force and average axial force are simulated as well. The resulting force field is then applied to the 3D FEM to induce deformation and to simulate tissue behavior to such applied force for different elastic moduli. Tissue deformation at different consecutive time frames is then picked up by using the B-mode imaging with the ultrasound transducer model implemented by Field II toolbox. The force is applied for about 1 msec. and the B-mode imaging procedure starts just after applying of the ARFI. Captured B-mode images resulting from imaging the wave propagation gives rise to an estimate of the shear wave speed (SWS) that is related to the tissue biomechanics.

The 2D pressure distribution is shown in Fig. 5. where the highest pressure value is observed around the preset focal point of 28.5 mm. Multiple transverse cross-sectional pressure distributions at different focal planes are shown in Fig. 6(a) where again the highest smoothest pressure distribution is observed at 33.35 mm which is the closest focal plane to the focal point. Pressure axial distribution at the focal beam (blue line) along with the averaged pressure axial distribution (red line) are shown in Fig. 6(b) where the peak axial pressure value is observed at 28.5 mm which is coincident with the preset focal point. Intensity axial distribution at the focal beam (blue line) along with averaged intensity axial distribution (red line) are shown in Fig. 6(c) where peak intensity axial value is observed at 28.5 mm. Acoustic axial force distribution at the focal beam (blue line) along with averaged force axial distribution (red line) are shown in Fig. 6(d) where acoustic force is calculated according to Eqn. (3):

$$F = \frac{2\alpha I}{C} \tag{3}$$

where $\alpha$ is the acoustic absorption coefficient in $(\frac{dB}{cm.MHz})$, $I$ is the temporal average intensity of the beam in $(\frac{Watts}{m^2})$, and $C$ is the speed of sound in tissue in $(\frac{m}{sec.})$.

### E. CORNEA SCATTERRER MODEL

FIELD II toolbox is used to generate the equivalent scatterrer model of the 3D FEM of cornea. The FEM consists of nodes with random spatial locations in-between and specific spatial locations at the boundaries. It is at these nodes where the ultrasound echoes are calculated to reconstruct an ultrasound line in the B-mode image. Nodes' spatial locations are exported to a comma separated value (csv) file with a fixed file structure; where x, y and z positions for each node are listed in single row. Each row is starting from the nodes' stationary spatial locations at the reference frame at the first three columns and the subsequent columns holds the nodes' new spatial locations at each time frame of simulation. Then we import this file to MATLAB for reading the scatterrers' spatial location at both the reference frame and each deformed frame in order to construct the B-mode image. A snapshot of corresponding file structure is presented in Table 4 where the presented spatial locations are x and z only as they are responsible for deformation in our FEM. The complete scatterrers model as seen by the ultrasound transducer is shown in Fig. 7.

## III. METHODOLOGY

Corneal biomechanics are estimated from the speed of propagating shear wave in response to acoustic radiation force impulse (ARFI) generated by the ultrasound transducer. This force impulse is generated by a focused ultrasound push and applied to the corneal tissue transiently for about 1 msec. ARFI causes deformation of corneal tissue as a wave propagating away from the focal point of application. The resulting deformation is then tracked using ultrasound transducer via high frame rate B-mode imaging procedure. Monitoring sequence is then obtained for the cornea model for complete 10 msec. of B-mode imaging resulting in a video stack for deformation propagation. Deformation is tracked in either direction laterally around the cornea apex by means of two fixed points in the video stack. One point is the focal point and the other one is laterally distal from cornea apex in either lateral direction. This process is repeated for different elastic moduli cornea models introduced in this study.

The proposed methodology is explained as follows:

i. 3D FEM, 2D scatterrer and ultrasound transducer models are implemented in parallel to simulate the average human cornea dimensions and linear array ultrasound transducer respectively, as discussed in section 2.1.
ii. The ultrasound transducer model is used to:

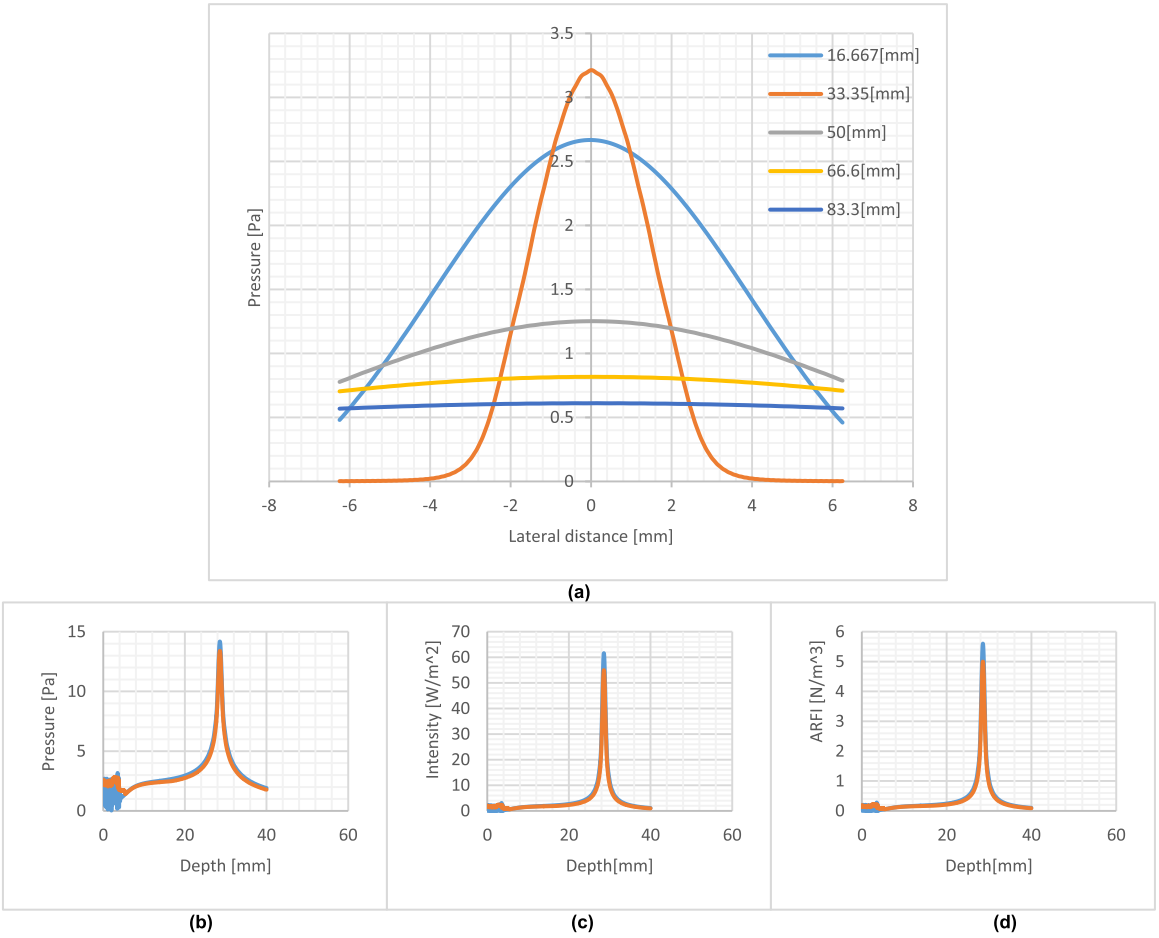


**FIGURE 6.** (a) multiple transverse cross-sectional pressure distributions at i. 16.6 mm (light blue), ii. 33.3 mm (orange), iii. 50 mm (gray), iv. 66.6 mm (yellow) and v. 83 mm (dark blue). (b) pressure axial distribution. (c) intensity distribution. (d) ARFI distribution.

**TABLE 4.** Scatterrer file snapshot.

| X | Z | u (mm) @ t=0 | v (mm) @ t=0 | u (mm) @ t=0.0174 | v (mm) @ t=0.0174 | : | : | : |
|---|---|---|---|---|---|---|---|---|
| -7.19115 | 0.647299 | 0 | 0 | -0.024530482 | -0.001285963 | : | : | : |
| -7.25 | 1.33E-15 | 0 | 0 | -0.006800931 | -0.003734764 | : | : | : |
| -8 | 1.47E-15 | 0 | 0 | 0 | 0 | : | : | : |
| -6.5 | 1.32E-15 | 0 | 0 | 0 | 0 | : | : | : |

a. Obtain a reference frame for the cornea before applying the ARFI (unloaded cornea frame).
b. Generate ARFI to act as internal stimulus for cornea tissue to deform.

iii. The generated ARFI is then applied to the 3D FEM to simulate the mechanical behavior of the cornea (loaded cornea) for different time frames corresponding to the frame rate of the ultrasound B-mode imaging. We use a frame rate of 100 KHz for high frame rate imaging procedures to reduce the error in the estimated values from ultrasound imaging, as discussed in section 2.3.
iv. The simulated time frames from the mechanical FEM model are then used to update the spatial locations of the scatterrers inside the scatterrer model.
v. The ultrasound transducer is used to image the updated scatterrer model to obtain different time frames.
vi. The corneal tissue biomechanics are estimated from the reference frame and the stack of deformed frames.
vii. This process is repeated for every cornea with elastic moduli included for this study.

### *A. ACQUISITION SEQUENCE*

Acquisition sequence starts by acquiring a reference frame for corneal tissue under study. This reference frame is acquired by transmitting a plane wave to the medium of interest (corneal tissue). Then an ARFI is sent to the corneal tissue for a short duration of time of about 1 msec. to resemble a transient force. This transient force is used to induce corneal tissue deformation giving rise to shear wave propagation

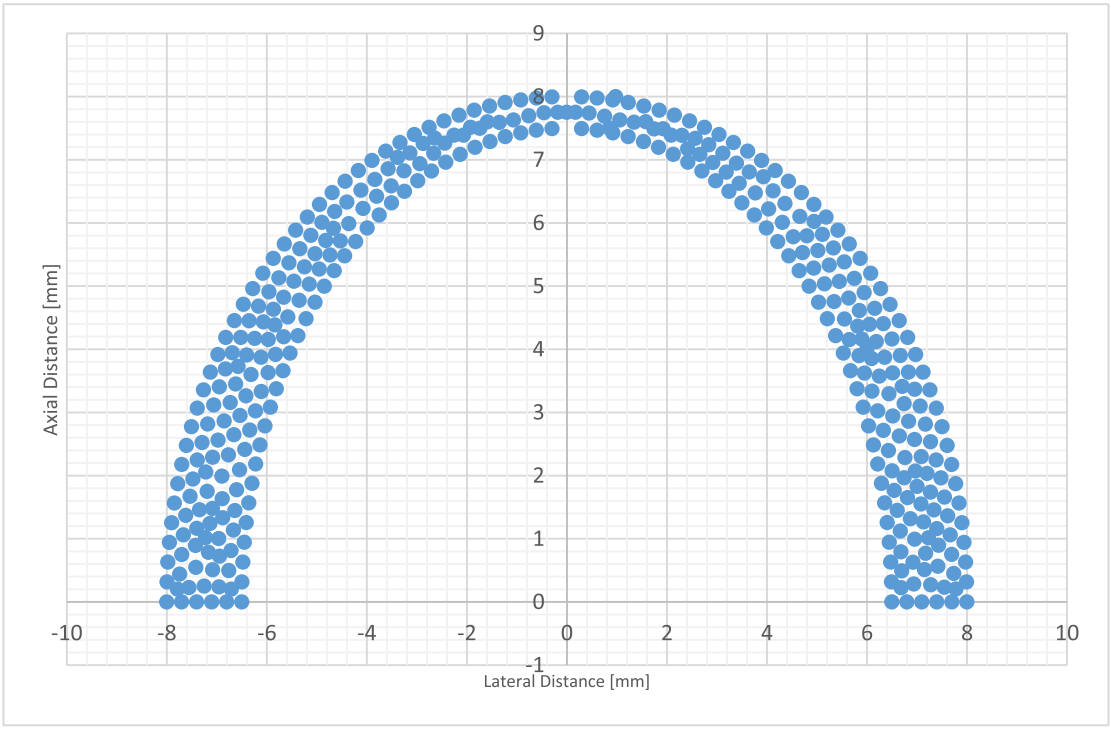


**FIGURE 7.** Complete human cornea scatterrer mode.

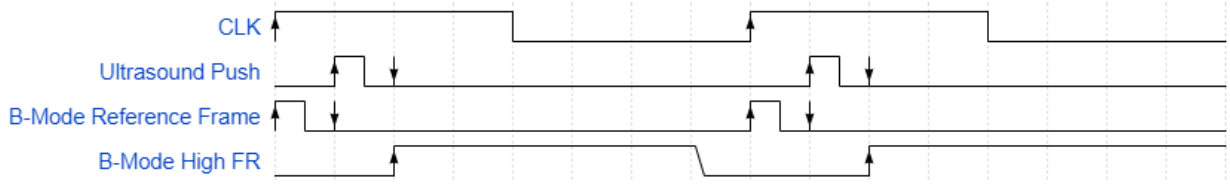


**FIGURE 8.** Timing diagram for two periods of the B-Mode acquisition sequence.

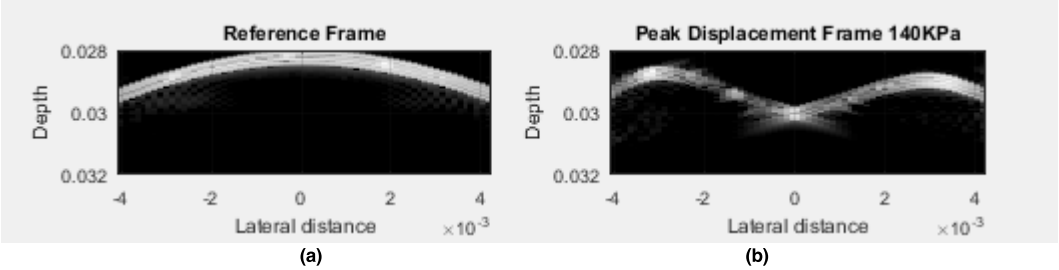


**FIGURE 9.** (a) Reference frame, (b) Peak deformation frame for cornea model.

inside the tissue. In this study we apply ARFI at a focal zone of 28.5 mm inside the tissue.

Just after applying of the ARFI to the corneal tissue, high frame rate B-mode imaging starts to capture the migrating shear wave in both lateral directions away from the focal zone. The frame rate used in this study is 100 KHz enabling the accurate tracking of the wave peak through acquisition time of 10 msec. The complete timing diagram for the complete B-mode imaging procedure is shown in Fig. 8. Apodization of the ultrasonic wave is performed to help reduce both the grating and side lobes of ultrasound beam.

### B. SHEAR WAVE SPEED ESTIMATION

Estimating shear wave speed is achieved by lateral Time-To-Peak displacement (lateral TTP) technique. The wave speed is estimated by dividing the lateral distance between the two probing nodes over the estimated times of wave peak arrival

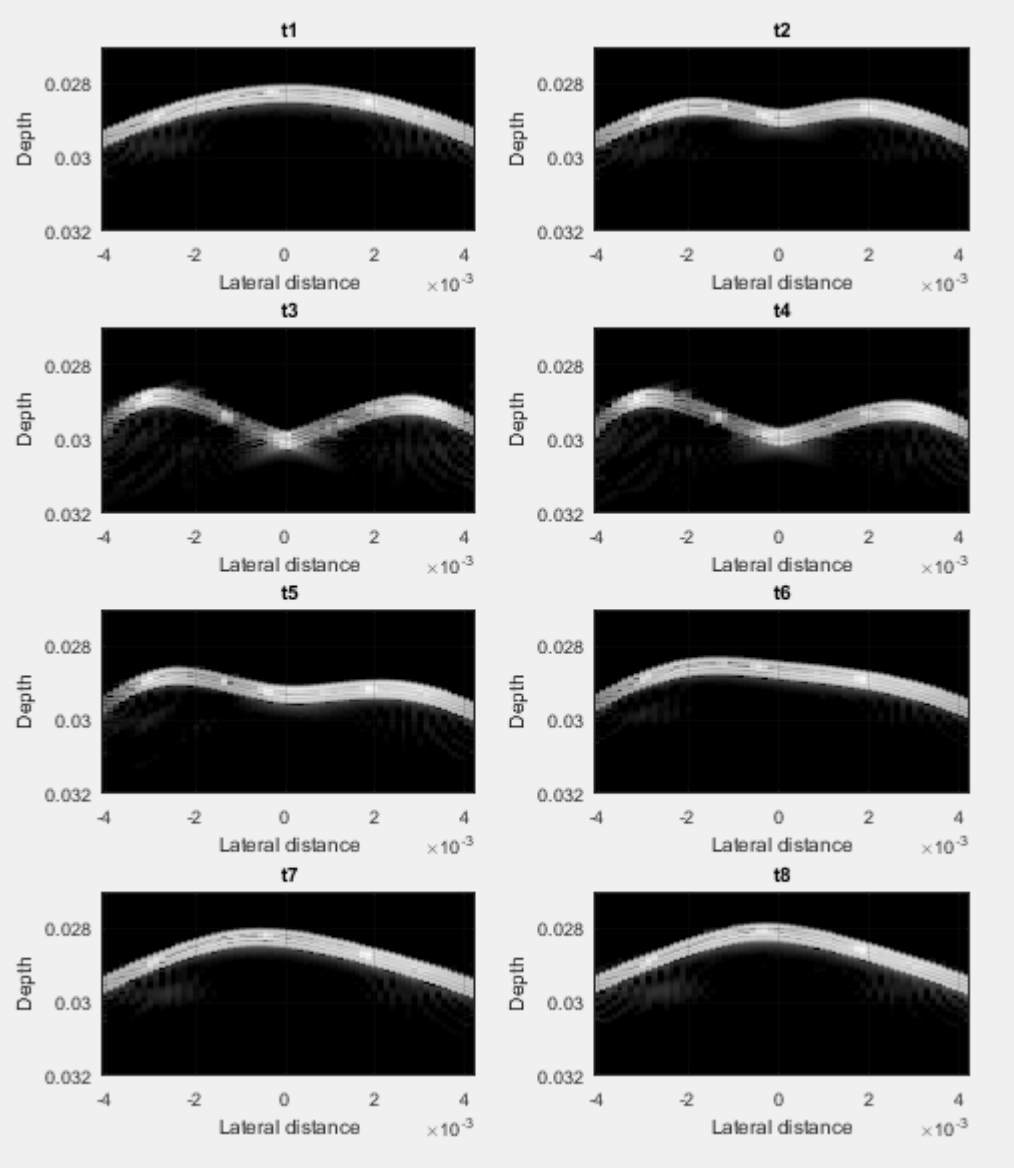


**FIGURE 10.** Shear wave deformed frames stack for 140KPa.

at these nodes. The two probing nodes are chosen to be the focal zones of two distal ultrasound beam, one node is at the focal zone of the central ultrasound beam and the other is at the focal zone of any of the lateral beams. The second probing point can be in either lateral direction as well, i.e. to the left or the right of the central beam. Time-To-Peak displacement is a property for every tissue biomechanics, where tissues with different elastic moduli yields different TTPs. It is worthy to be noted that, dependence on ARFI value only changes the amplitude of tissue deformation where two different elastic moduli tissues having same ARFI value will yield two different peak deformation values. Moreover, these two tissues will yield two different TTP values. TTP is estimated for tissue under study from displacement curve obtained for the probing node with proper tracking frequency considerations. Equation (4) is used to calculate the estimated SWS:

$$C_{avg} = \frac{\Delta x}{\Delta t} \tag{4}$$

where $C_{avg}$ is the average velocity across the lateral position, $\Delta x$ and $\Delta t$ are the difference in distance between probing nodes and difference in times of peak arrival at these nodes respectively.

## IV. RESULTS

Figure 9 shows the reference frame and peak axial deformation frame after applying ARFI for 140 KPa corneal model. The focal point is observed to reach its peak deformation along the axial direction in Fig. 9 (b). These two figures are

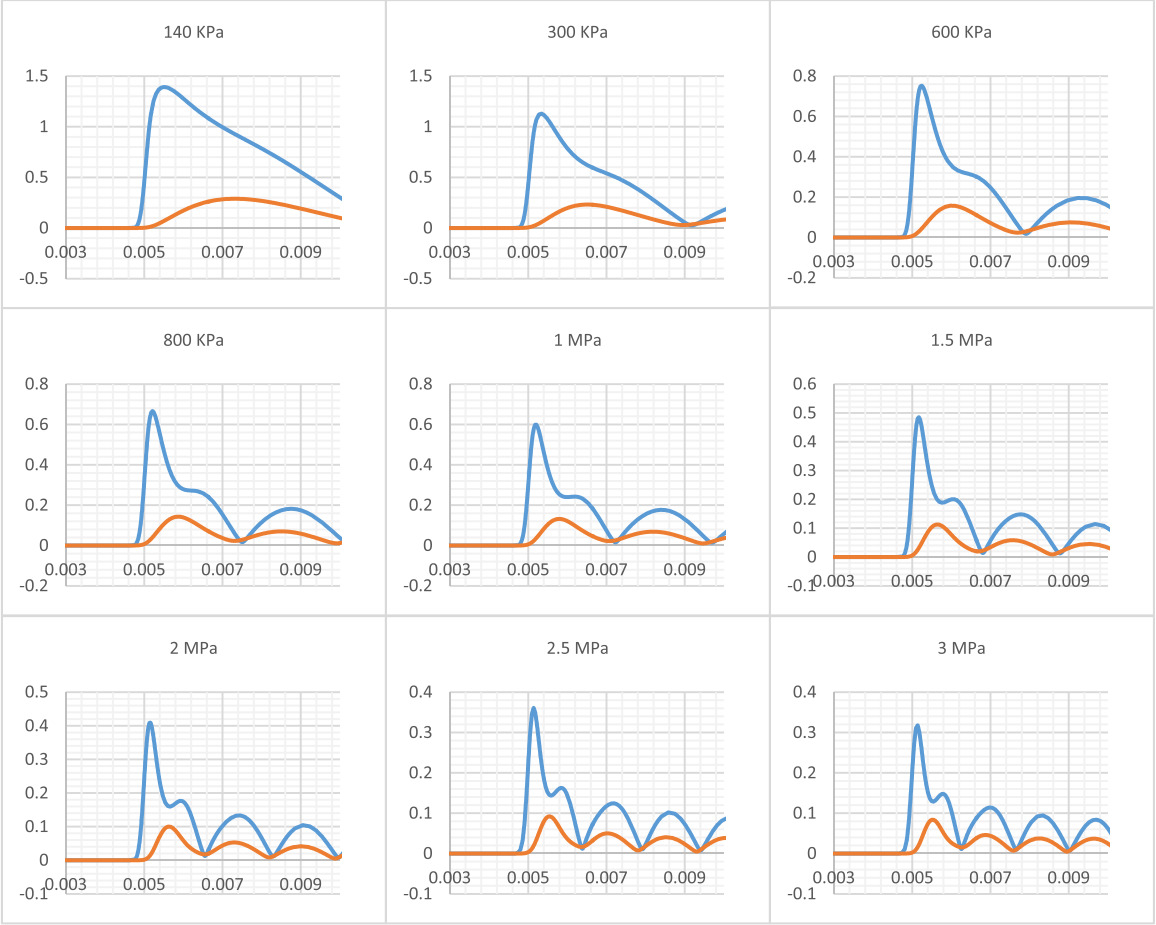


**FIGURE 11.** 1D Deformation profiles for focal and lateral probed nodes for each cornea model (Blue line = focal node displacement, Red line = radial node displacement).

chosen for illustration purposes, where all other different elastic moduli models included in this research have undergone the same procedure and yielded the relevant outcomes.

The reference frame shown in Fig. 9(a) is used as a base for estimating the axial deformation of the cornea through subsequent time frames after applying ARFI, and estimating the peak axial deformation as well. It is considered the starting point in transient elastography imaging procedure. This reference frame is obtained for all cornea models with different elastic moduli namely; 140 KPa, 300 KPa, 600 KPa, 800 KPa, 1 MPa, 1.5 MPa, 2 MPa, 2.5 MPa and 3 MPa. The field of view (FOV) is limited to the lateral distance obtained by the ultrasound probe during B-mode imaging. The field of view (FOV) in this experiment is about 8 mm in the lateral direction and about 12 mm in the axial direction. Cornea tissue is observed to occupy axial location from 28 mm to 28.5 mm at the apex which is relevant to literature information about corneal thickness at the apex to be about 0.5 mm.

Peak corneal deformation after applying ARFI is shown in Fig. 9 (b) where the 8 mm wide FOV is considered to be optimum for monitoring the lateral deformation of the cornea. This is an empirical result obtained by try and error. The shear wave is observed at this frame clearly, where it propagates in either lateral direction along the corneal tissue.

A complete simulation for shear wave propagation inside corneal model of 140 KPa along the temporal domain is performed and shown in Fig. 10. Shear wave propagation is shown for only eight different time stamps along with the reference frame at the beginning for convenience in presentation. The monitoring sequence starts with the reference frame at 0 sec. before which ARFI is applied and end up at 10 msec.

A complete simulation time sequence with 100 KHz frame for each corneal model is obtained. The deformation along these frames is tracked at each time frame and compared with the reference frame. Complete 1D deformation curves for both the focal point and the lateral point are then constructed from the peak deformation tracking procedure and are shown in Fig. 11. The time axis starts from 3 msec. to 10 msec. and not from 0 sec. since there are no significant information before deformation to be shown along the curve.

Figure 12 shows the estimated times at which focal peak deformation takes place for each corneal model. These times enables the estimation for the frame at which the peak deformation happens, hence enabling the estimation of

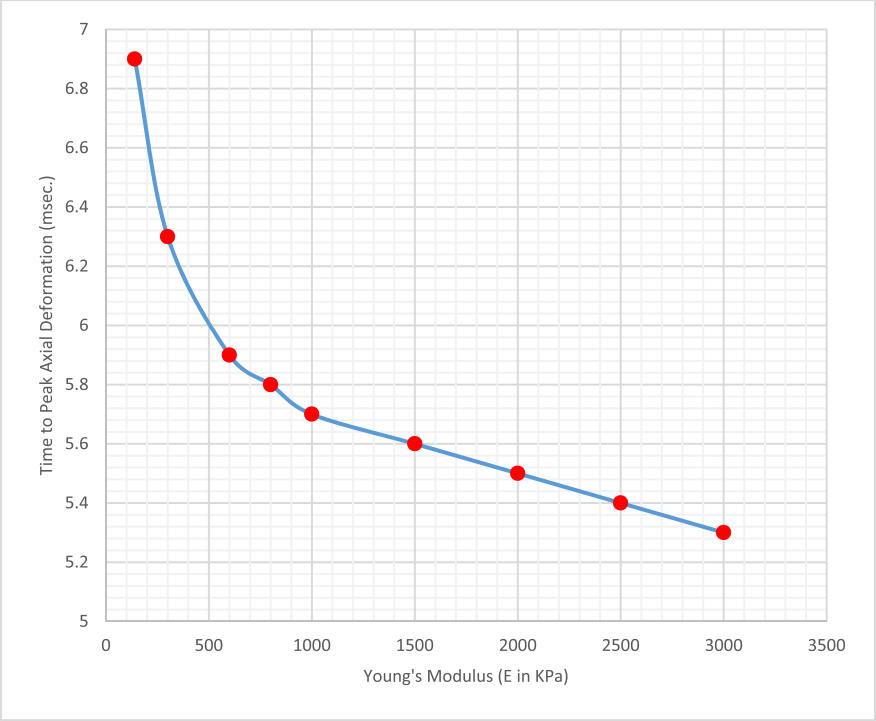


**FIGURE 12.** Time-To-Peak (TTP) deformation for each cornea model.

the focal peak deformation itself accurately (Deformation Amplitude). This is achieved by means of the reference frame and the estimated peak deformation frame. Reference frame along with peak deformation frame for each corneal model is shown in Fig. 13. These frames are used to estimate the peak deformation value for each cornea model and the Deformation Amplitude Ratio at 2 mm in either lateral direction distal from the apex as well.

1D deformation curves allow for estimating the SWS for each cornea model by calculating the time difference between TTPs for each of the two probing nodes divided by their spatial distance. Theoretical, estimated shear wave speed along with speed estimation accuracy for each cornea model are listed in Table 5.

Deformation amplitude is estimated accurately for each cornea model by comparing the ultrasound B-mode focal beam for the reference frame and corresponding deformation frame. The reference beam along with all deformed beams for each cornea model are presented in Fig. 14. The deformation amplitude is considered to be the difference between the axial location at which the cornea tissue appears and the axial location at which each other cornea tissue for different cornea models appear. The deformation amplitudes are shown in Fig. 15.

Figure 16 shows the deformation amplitude ratios for each elastic modulus cornea model. They are estimated from B-mode images where the focal peak axial deformation happens. It is the ratio between the apex deformation to 2 mm nasal or temporal peak axial deformation. Deformation amplitude ratio defines how the cornea apex deforms with respect to either 1 mm or 2 mm nasal or temporal deformation of corneal tissue.

## V. DISCUSSION

From Fig. 10. it is observed that corneal tissue experiences one complete cycle of wave propagation within 10 msec. at 140 KPa. The higher the elastic modulus for cornea tissue the higher the number of cycles of wave propagation. It is observed also that 140 KPa reaches its peak deformation at t3 when applying ARFI. The tissue starts by no deformation at the beginning of the simulation and deformation increases gradually till its peak value and then dampens again till reaching the no deformation state again. Many periods of ARFI application can be performed to obtain an average tissue behavior and more accurate results for biomechanical parameters.

TTP values for focal peak axial displacements shows a TTP value of 6.9 msec. at 140 KPa and 5.3 msec. at 3 MPa with time difference in TTPs between 140 KPa and 3 MPa of 1.6 msec. This narrow time difference makes it nearly impossible to estimate the corneal tissue biomechanics with ordinary ultrasound transducers operating with nearly several tens or even hundreds of frame rate. Yet, it is possible to achieve optimum temporal resolution with transducers operating with several thousand or even hundreds of thousands frame rate as in this study. In this study, 100 KHz frame rate gives about 160 frames for the 1.6 msec. time difference between TTPs of 140 KPa and 3 MPa, which is optimum

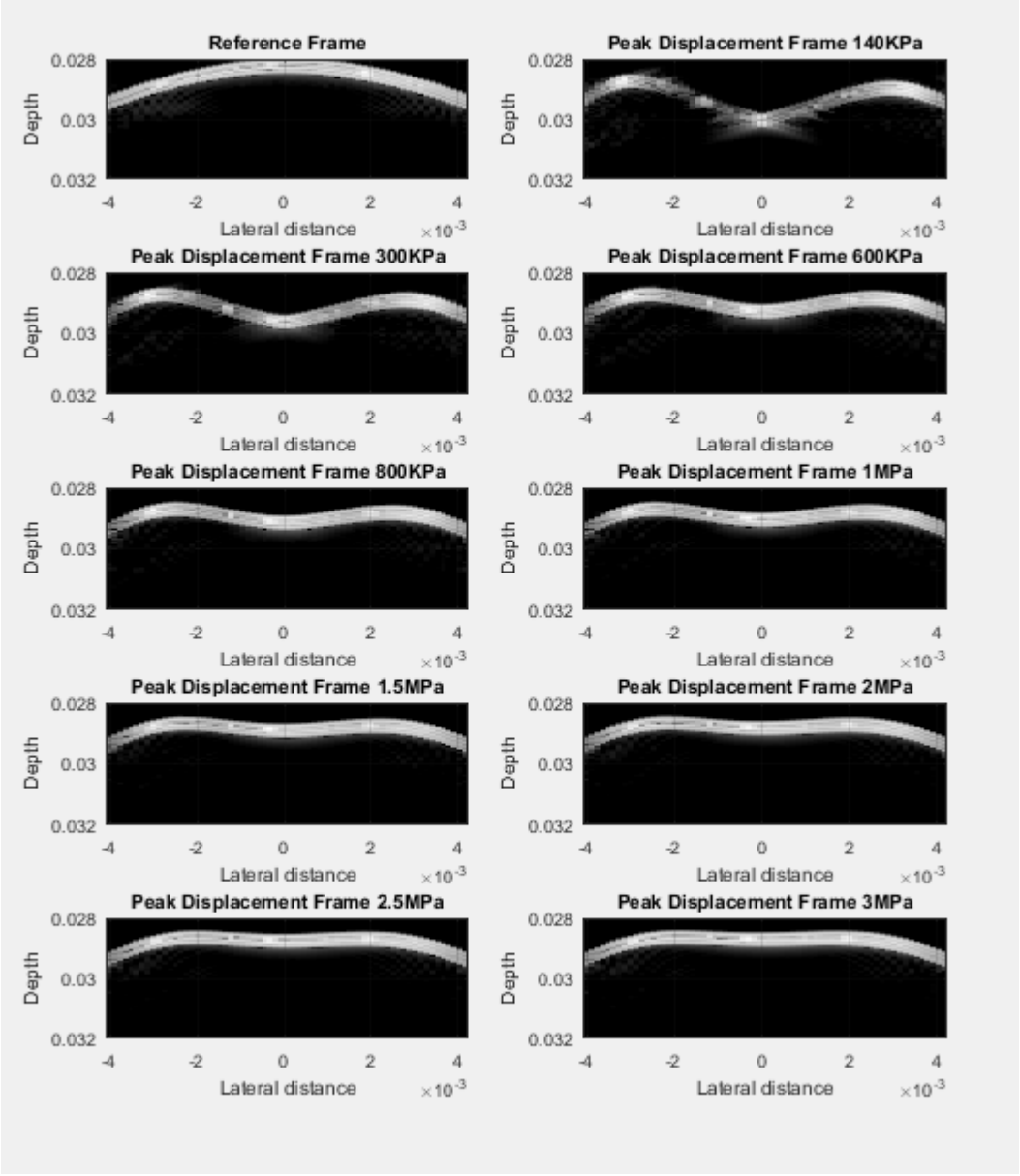


**FIGURE 13.** Reference frame along with peak deformation frame for each cornea model.

**TABLE 5.** Theoretical, estimated SWS and accuracy for each cornea model.

| Young's Modulus (Pa) | Theoretically (m/sec.) | Estimated (m/sec.) @ 100 KHz | Accuracy (%) |
|---|---|---|---|
| 140K | 7.157217283 | 7.142857143 | 99.79936 |
| 300K | 10.4770933 | 10.34482759 | 98.73757 |
| 600K | 14.81684744 | 14.63414634 | 98.76694 |
| 800K | 17.10902172 | 17.14285714 | 99.80224 |
| 1M | 19.1284678 | 18.75 | 98.02144 |
| 1.5M | 23.42749283 | 23.07692308 | 98.5036 |
| 2M | 27.05173859 | 26.42857143 | 97.69639 |
| 2.5M | 30.24476319 | 30 | 99.19073 |
| 3M | 33.1314781 | 33.33333333 | 99.39074 |

to differentiate between them. TTP decrease as elasticity of tissue increases as shown in Fig. 12.

From Fig. 11 and Fig. 13 it is observed that force is dampened rapidly in temporal domain and spatial domain,

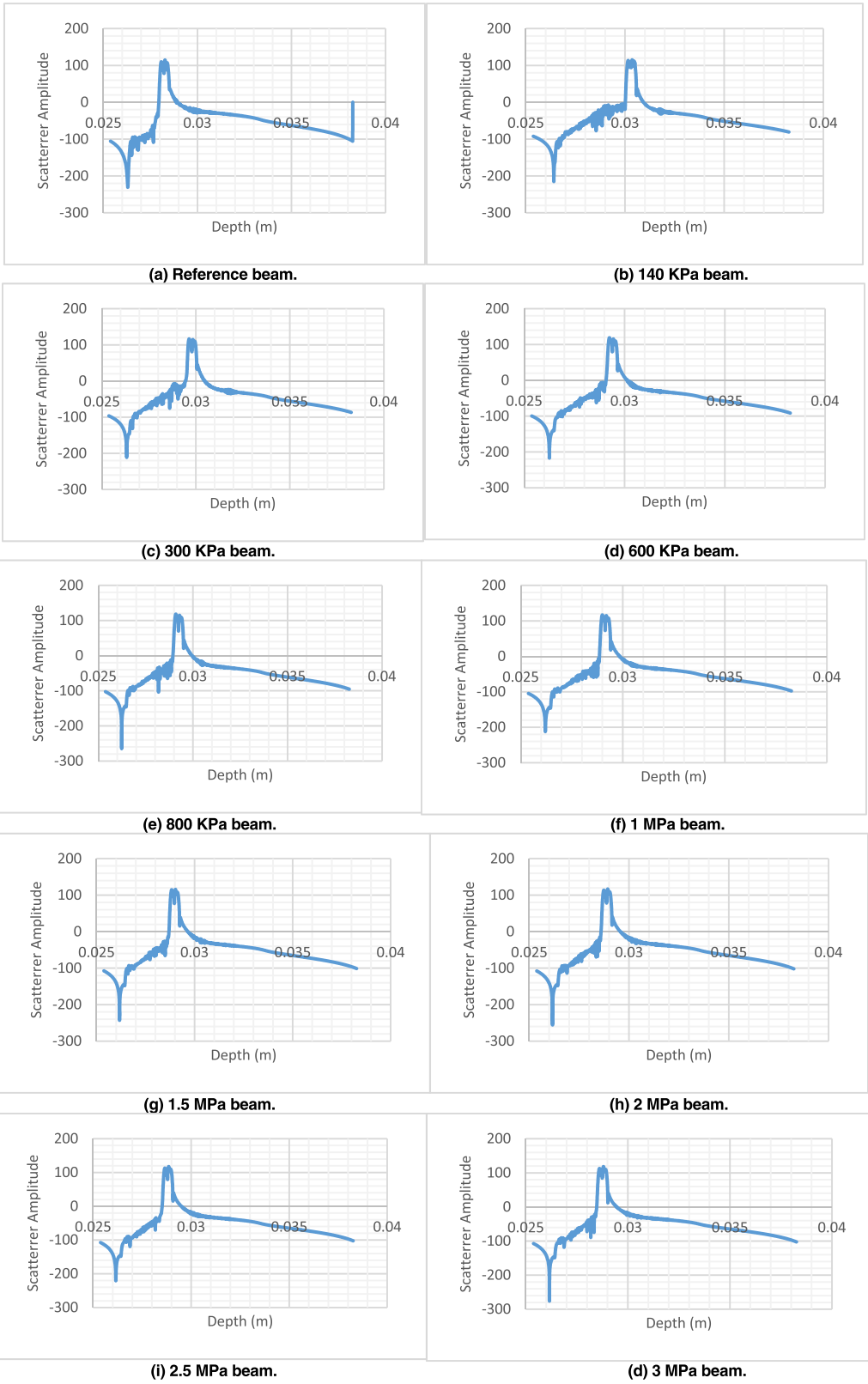


**FIGURE 14.** Reference beam along with all deformed beams for each cornea model.

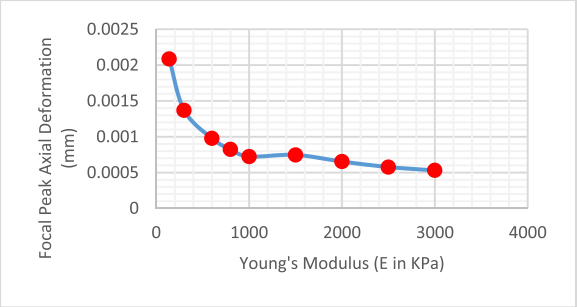


**FIGURE 15.** Deformation amplitude for each cornea model.

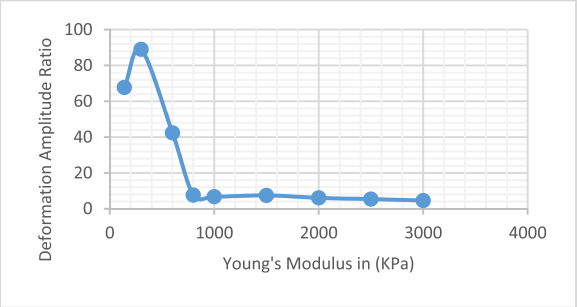


**FIGURE 16.** Deformation amplitude ratio for each cornea model.

where complete B-mode frame shows high localization of the force around the point of application, and deformation curves shows the rapid dampening in time for force after time of application.

From Fig. 15. We observed that deformation amplitudes decrease as the Young's modulus increase for corneal models. As elastic moduli shift to MPa range the difference between two consecutive deformation amplitudes becomes smaller. Differentiation between these deformation amplitudes is subjected to transducer axial resolution. Lateral resolution affects only the shear wave tracking process in the lateral direction, where the probing nodes are fixed with beam width. As beam width determines lateral resolution of the transducer, hence determining the lateral distance between the probing nodes. Smaller lateral distance yields worse temporal resolution between deformation curves of the two probing nodes of the wave speed, while larger lateral distance yields better temporal resolution.

We conclude from Fig. 14. that transducer's axial resolution is capable of differentiating between four of the major corneal layers.

Our estimation accuracy of SWS was maximum at 800 KPa with value of 99.8% and minimum at 2 MPa with value of 97.6% with respect to the theoretical SWS calculated from Eqn. (1).

As shown in Fig. 16. DA ratio at 2 mm represents how cornea apex deforms with respect to paracentral regions. It is observed that cornea models with low elastic modulus have high DA ratio values while DA ratio value decreases as the elastic modulus increases which is matching with experimental results obtained in relevant studies. DA ratio gives an objective information about how whole corneal tissue deforms in response to ARFI or any external force. This means that for corneal pre-refractive surgery; where its stiffness is considered to be high; DA ration at 2 mm is supposed to be small. While cornea post-refractive surgery is supposed to have high DA ratio at 2 mm as its stiffness is considered to be decreased by the surgery.

If we depend only on one of the estimated parameters for estimating the corneal biomechanics is not recommended. This is due to the misleading estimation as in the case of 300 KPa cornea model, where the estimated deformation amplitude ratio at 2mm value is supposed to be smaller than that of 140 KPa, while the estimated value is observed to be higher. Depending only on deformation amplitude ratio at 2 mm value supposes that the estimated corneal elastic modulus should be lower than that of 140 KPa. However, depending on all the estimated parameters values assessing corneal biomechanics leads to accurate estimation of corneal biomechanics and accurate assessment of post-refractive surgery.

## VI. CONCLUSION

In this research, shear wave speed, deformation amplitude, Time-To-Peak deformation and deformation amplitude ratio for different elastic moduli cornea models are estimated respectively. Two models are used in parallel to study the behavior of cornea biomechanics pre- and post-refractive surgery, namely, FEM in conjunction with scatterrer model. Third ultrasound transducer model is used to simulate the behavior of ultrasound transducer while imaging corneal tissue undergoing transient elastography. Also, the transducer model is used to simulate the transducer behavior while generating acoustic radiation force impulse that is used to excite corneal tissue. Nine FEMs are used to represent cornea in different biomechanical states pre- and post-refractive, 140 KPa, 300 KPa, 600 KPa and 800 KPa as post-refractive surgery corneal models and 1 MPa, 1.5 MPa, 2 MPa, 2.5 MPa and 3 MPa as pre-refractive surgery corneal models.

ARFI is applied transiently to each of the nine cornea models to induce deformation wave propagation. This wave of tissue deformation is tracked using B-mode imaging procedure that yields a video stack for each cornea model representing the wave propagation. The B-mode video stack including deformation wave is tracked by a 100 KHz frame rate. Resulting wave speed is tracked through two fixed probing points assigned on two fixed ultrasound beams, one point is at cornea apex, and the other is distal from cornea apex in either lateral direction. Number of probing points is subjected to the lateral resolution of the transducer, where involving more probing points inside the B-mode image frame means finer lateral resolution of the utilized transducer.

Focal TTP deformation values are estimated from TTP deformation curves for the focal apical probing point. It is

observed that increasing corneal stiffness yields decrease in TTP deformation values.

Focal peak axial deformations are estimated from focal ultrasound beams by estimating corneal tissue axial location in both the reference frame and all peak deformation frames for each cornea model. Deformation amplitude values are observed to be decreasing by increase in corneal stiffness.

Similarly, paracentral axial deformations are estimated which enabled the estimation of deformation amplitude ration at 2 mm. Deformation amplitude ratios at 2 mm are shown to be decreasing with increasing the elastic modulus of the corneal tissue.

Shear wave speed values are estimated using the TTP deformation curves for both probing points. Lateral distance between the probing points divided by peaks arrival times gives an estimate to the corresponding shear wave speed of the cornea model under study. Elastic moduli can be estimated from the resulting shear wave speeds as they are related by Eqn. (4).

It is recommended to depend on each of the estimated parameters values of TTP deformation, deformation amplitude, deformation amplitude ratio at 2 mm and shear wave speed respectively when assessing cornea biomechanics post refractive surgery. Depending only on one of these values may be misleading and vague. As in the case of 300 KPa cornea model.

## REFERENCES


[1] A. Elsheikh, D. Wang, M. Brown, P. Rama, M. Campanelli, and D. Pye, "Assessment of corneal biomechanical properties and their variation with age," *Current Eye Res.*, vol. 32, no. 1, pp. 11–19, Jan. 2007, doi: 10.1080/02713680601077145.

[2] I. Fatt and B. A. Weissman, *Physiology of the Eye: An Introduction to the Vegetative Functions*. Oxford, U.K.: Butterworth-Heinemann, 2013.

[3] R. Vinciguerra, S. Rehman, N. A. Vallabh, M. Batterbury, G. Czanner, A. Choudhary, R. Cheeseman, A. Elsheikh, and C. E. Willoughby, "Corneal biomechanics and biomechanically corrected intraocular pressure in primary open-angle glaucoma, ocular hypertension and controls," *Brit. J. Ophthalmol.*, vol. 104, no. 1, pp. 121–126, Jan. 2020, doi: 10.1136/bjophthalmol-2018-313493.

[4] F. Bao, B. Geraghty, Q. Wang, and A. Elsheikh, "Consideration of corneal biomechanics in the diagnosis and management of keratoconus: Is it important?" *Eye Vis.*, vol. 3, no. 1, pp. 1–6, Dec. 2016, doi: 10.1186/s40662-016-0048-4.

[5] R. Ambrósio, B. T. Lopes, F. Faria-Correia, M. Q. Salomão, J. Bühren, C. J. Roberts, A. Elsheikh, R. Vinciguerra, and P. Vinciguerra, "Integration of scheimpflug-based corneal tomography and biomechanical assessments for enhancing ectasia detection," *J. Refractive Surg.*, vol. 33, no. 7, pp. 434–443, Jul. 2017, doi: 10.3928/1081597X-20170426-02.

[6] R. Dou, Y. Wang, L. Xu, D. Wu, W. Wu, and X. Li, "Comparison of corneal biomechanical characteristics after surface ablation refractive surgery and novel lamellar refractive surgery," *Cornea*, vol. 34, no. 11, pp. 1441–1446, Nov. 2015, doi: 10.1097/ICO.0000000000000556.

[7] W. J. Dupps and S. E. Wilson, "Biomechanics and wound healing in the cornea," *Experim. Eye Res.*, vol. 83, no. 4, pp. 709–720, Oct. 2006, doi: 10.1016/j.exer.2006.03.015.

[8] I. Schmack, D. G. Dawson, B. E. McCarey, G. O. Waring, H. E. Grossniklaus, and H. F. Edelhauser, "Cohesive tensile strength of human LASIK wounds with histologic, ultrastructural, and clinical correlations," *J. Refractive Surg.*, vol. 21, no. 5, pp. 433–445, Sep. 2005.

[9] T. Seiler and A. W. Quurke, "Iatrogenic keratectasia after LASIK in a case of forme fruste keratoconus," *J. Cataract Refractive Surg.*, vol. 24, pp. 1007–1009, Jul. 1998.

[10] J. Liu and C. J. Roberts, "Influence of corneal biomechanical properties on intraocular pressure measurement: Quantitative analysis," *J. Cataract Refractive Surg.*, vol. 31, no. 1, pp. 146–155, 2005.

[11] N. Malik, S. Moss, N. Ahmed, A. Furth, R. Wall, and K. Meek, "Ageing of the human corneal stroma: Structural and biochemical changes," *Biochim. et Biophys. Acta (BBA) Mol. Basis Disease*, vol. 1138, no. 3, pp. 222–228, Mar. 1992.

[12] A. Kanai, "Electron microscopic studies of corneal stroma: Aging changes of collagen fibers," *Ann. Ophthalmol.*, vol. 5, no. 3, pp. 285–287, 1973.

[13] A. Daxer, K. Misof, B. Grabner, A. Ettl, and P. Fratzl, "Collagen fibrils in the human corneal stroma: Structure and aging," *Investig. Ophthalmol. Vis. Sci.*, vol. 39, no. 3, pp. 644–648, 1998.

[14] I. G. Pallikaris, G. D. Kymionis, H. S. Ginis, G. A. Kounis, and M. K. Tsilimbaris, "Ocular rigidity in living human eyes," *Investig. Ophthalmol. Vis. Sci.*, vol. 46, no. 2, pp. 409–414, 2005.

[15] J. Ytteborg, "Further investigations of factors influencing size of rigidity coefficient," *Acta Ophthalmolog.*, vol. 38, no. 6, pp. 643–657, May 2009.

[16] A. S. Roy, W. J. Dupps, and C. J. Roberts, "Comparison of biomechanical effects of small-incision lenticule extraction and laser *in situ* keratomileusis: Finite-element analysis," *J. Cataract Refractive Surg.*, vol. 40, no. 6, pp. 971–980, 2014.

[17] D. Wu, Y. Wang, L. Zhang, S. Wei, and X. Tang, "Corneal biomechanical effects: Small-incision lenticule extraction versus femtosecond laser–assisted laser *in situ* keratomileusis," *J. Cataract Refractive Surg.*, vol. 40, no. 6, pp. 954–962, Jun. 2014, doi: 10.1016/j.jcrs.2013.07.056.

[18] A. H. Vestergaard, K. T. Grønbech, J. Grauslund, A. R. Ivarsen, and J. Ø. Hjortdal, "Subbasal nerve morphology, corneal sensation, and tear film evaluation after refractive femtosecond laser lenticule extraction," *Graefe's Arch. Clin. Experim. Ophthalmol.*, vol. 251, no. 11, pp. 2591–2600, Nov. 2013.

[19] R. Shah, S. Shah, and S. Sengupta, "Results of small incision lenticule extraction: All-in-one femtosecond laser refractive surgery," *J. Cataract Refractive Surg.*, vol. 37, no. 1, pp. 127–137, 2011.

[20] A. Vestergaard, A. R. Ivarsen, S. Asp, and J. Ø. Hjortdal, "Small-incision lenticule extraction for moderate to high myopia: Predictability, safety, and patient satisfaction," *J. Cataract Refractive Surg.*, vol. 38, no. 11, pp. 2003–2010, 2012.

[21] F. Al-Tobaigy, "Efficacy, predictability, and safety of laser-assisted subepithelial keratectomy for the treatment of myopia and myopic astigmatism," *Middle East Afr. J. Ophthalmol.*, vol. 19, no. 3, p. 304, 2012.

[22] M. A. Qazi, J. P. Sanderson, A. M. Mahmoud, E. Y. Yoon, C. J. Roberts, and J. S. Pepose, "Postoperative changes in intraocular pressure and corneal biomechanical metrics: Laser *in situ* keratomileusis versus laser-assisted subepithelial keratectomy," *J. Cataract Refractive Surg.*, vol. 35, no. 10, pp. 1774–1788, 2009.

[23] J. Bercoff, M. Tanter, L. Sandrin, S. Catheline, and M. Fink, "Ultrafast compound imaging for 2D displacement vector measurements: Application to transient elastography and color flow mapping," in *Proc. IEEE Ultrason. Symp.*, vol. 2, Oct. 2001, pp. 1619–1622, doi: 10.1109/ultsym.2001.992032.

[24] J. Bercoff, M. Tanter, and M. Fink, "Supersonic shear imaging: A new technique for soft tissue elasticity mapping," *IEEE Trans. Ultrason., Ferroelectr., Freq. Control*, vol. 51, no. 4, pp. 396–409, Apr. 2004, doi: 10.1109/TUFFC.2004.1295425.

[25] J. Bercoff, S. Chaffai, M. Tanter, L. Sandrin, S. Catheline, M. Fink, J. L. Gennisson, and M. Meunier, "*In vivo* breast tumor detection using transient elastography," *Ultrasound Med. Biol.*, vol. 29, no. 10, pp. 1387–1396, 2003, doi: 10.1016/S0301-5629(03)00978-5.

[26] M. L. Palmeri, M. H. Wang, J. J. Dahl, K. D. Frinkley, and K. R. Nightingale, "Quantifying hepatic shear modulus *in vivo* using acoustic radiation force," *Ultrasound Med. Biol.*, vol. 34, no. 4, pp. 546–558, Apr. 2008, doi: 10.1016/j.ultrasmedbio.2007.10.009.

[27] M. Tanter, D. Touboul, J. L. Gennisson, J. Bercoff, and M. Fink, "High-resolution quantitative imaging of cornea elasticity using supersonic shear imaging," *IEEE Trans. Med. Imag.*, vol. 28, no. 12, pp. 1881–1893, Dec. 2009, doi: 10.1109/TMI.2009.2021471.

[28] H. M. Ahmed, N. M. Salem, A. F. Seddik, and M. I. El-Adawy, "Investigating relationship between lateral time-to-peak (TTP) displacement curves and stiffness of viscoelastic agar-gelatin phantoms," in *Proc. Int. Conf. Innov. Trends Comput. Eng. (ITCE)*, Feb. 2019, pp. 35–40, doi: 10.1109/ITCE.2019.8646388.

[29] L. Crocetti, F. Calcagni, G. Gherarducci, N. Tosoratti, C. Amabile, F. P. Tarantino, I. Bargellini, S. Cassarino, R. Cioni, and D. Caramella, "Monitoring of thermal-induced changes in liver stiffness during controlled hyperthermia and microwave ablation in an *ex vivo* bovine model using point shear wave elastography," *CardioVascular Interventional Radiol.*, vol. 42, no. 5, pp. 744–750, May 2019, doi: 10.1007/s00270-018-02152-y.
[30] H. Li, J. Porée, M.-H. R. Cardinal, and G. Cloutier, "Two-dimensional affine model-based estimators for principal strain vascular ultrasound elastography with compound plane wave and transverse oscillation beamforming," *Ultrasonics*, vol. 91, pp. 77–91, Jan. 2019, doi: 10.1016/j.ultras.2018.07.012.
[31] C. Rabin and N. Benech, "Quantitative breast elastography from b-mode images," *Med. Phys.*, vol. 46, no. 7, pp. 3001–3012, 2019, doi: 10.1002/mp.13537.
[32] J. Racedo and M. W. Urban, "Evaluation of reconstruction parameters for 2-D comb-push ultrasound shear wave elastography," *IEEE Trans. Ultrason., Ferroelectr., Freq. Control*, vol. 66, no. 2, pp. 254–263, Feb. 2019, doi: 10.1109/TUFFC.2018.2884348.
[33] A. J. Sit, S.-C. Lin, A. Kazemi, J. W. McLaren, C. M. Pruet, and X. Zhang, "*In vivo* noninvasive measurement of Young's modulus of elasticity in human eyes: A feasibility study," *J. Glaucoma*, vol. 26, no. 11, pp. 967–973, Nov. 2017, doi: 10.1097/IJG.0000000000000774.
[34] A. Elsheikh, D. Wang, and D. Pye, "Determination of the modulus of elasticity of the human cornea," *J. Refractive Surg.*, vol. 23, no. 8, pp. 808–818, Oct. 2007, doi: 10.3928/1081-597x-20071001-11.
[35] X. Qin, L. Tian, H. Zhang, X. Chen, and L. Li, "Evaluation of corneal elastic modulus based on corneal visualization scheimpflug technology," *Biomed. Eng. OnLine*, vol. 18, no. 1, p. 42, Dec. 2019, doi: 10.1186/s12938-019-0662-1.
[36] D. G. Dawson, R. J. Ambrosio, and W. B. Lee, "Corneal biomechanics: Basic science and clinical applications," *Focal Point*, vol. 34, pp. 3–8, 2016.
[37] R. Ambrósio, R. S. Alonso, A. Luz, and L. G. Coca Velarde, "Corneal-thickness spatial profile and corneal-volume distribution: Tomographic indices to detect keratoconus," *J. Cataract Refractive Surg.*, vol. 32, no. 11, pp. 1851–1859, Nov. 2006, doi: 10.1016/j.jcrs.2006.06.025.
[38] M. Flannigan, D. Jehle, and J. Wilson. *Radiology KeyFastest Radiology Insight Engine*. Accessed: Jun. 12, 2021. [Online]. Available: https://radiologykey.com/eye-emergencies/

**HASSAN M. AHMED** was born in Egypt, in 1989. He received the B.Sc. and M.Sc. degrees in biomedical engineering from Helwan University, Cairo, Egypt, in 2012 and 2016, respectively, where he is currently pursuing the Ph.D. degree in biomedical engineering. His current research interests include elastography, soft tissue shear wave estimation, biomechanics, signal processing, medical image processing, machine learning, electromagnetics, and dual band RF coils for ultrahigh MRI.

**WALID AL-ATABANY** received the B.Sc. and M.Sc. degrees from the Biomedical Engineering Department, Cairo University, in 1999 and 2004, respectively, and the Ph.D. degree in biomedical engineering from Imperial College London, in 2010. In 2011, he was a Research Associate with Newcastle University, for two years. He is currently a Full Professor with the Information Technology and Computer Science School, Nile University. He has over 50 publications in highly impacted journals and conferences. His research interests include highly interdisciplinary, however, the main interest focuses in the area of assistive techniques for visually impaired and prosthetic vision. Also his research extended to include problems related to advancement of statistical signal and image processing, as well as machine learning methods (including deep learning) and their application to large-scale pattern classification and signal interpretation problems (e.g., EEC and ECG signals). He received the 2nd Price Award from the 2nd Symposium of the Neuroscience Technology Network (NTN2009), the ARVO 2010 travel grant from the AFER/National Institute for Health Research Centre for Ophthalmology, and the two Newton institutional link grants from the British council, in 2015 and 2016, respectively.

**NANCY M. SALEM** received the B.Sc. and M.Sc. degrees in electronics and communications engineering from Helwan University, Cairo, Egypt, in 1998 and 2003, respectively, and the Ph.D. degree in engineering from the Department of Electrical Engineering and Electronics, University of Liverpool, U.K., in 2007. In 2008, she joined the Department of Electronics and Communications Engineering, Helwan University, as an Assistant Professor, where she is currently a Professor with the Department of Biomedical Engineering. Her current research interests include signal processing, medical image processing, machine learning, deep learning, and modeling. She was a member with the Institute of Electrical and Electronics Engineers and the Counselor of the Women in Engineering (WIE) and IEEE Helwan Student Branch. She reviewed many scientific articles, proposals, and research projects.